Received: 2 May 2024 | Revised: 4 July 2024 | Accepted: 5 July 2024

DOI: 10.1002/ardp.202400337

ARCH PHARM DPhG
Archiv der Pharmazie

FULL PAPER

New potent muscarinic receptor ligands bearing the 1,4-dioxane nucleus: Investigation on the nature of the substituent in position 2

Gianfabio Giorgioni[1] | Alessandro Bonifazi[2] | Rosanna Matucci[3] | Federica Matteucci[1] | Alessandro Piergentili[1] | Alessia Piergentili[1] | Wilma Quaglia[1] | Silvia Gervasoni[4,5] | Giulio Vistoli[4] | Serena Vittorio[4] | Fabio Del Bello[1]

[1]Scuola di Scienze del Farmaco e dei Prodotti della Salute, Università degli Studi di Camerino, Camerino, Italy

[2]Medicinal Chemistry Section, Molecular Targets and Medications Discovery Branch, National Institute on Drug Abuse—Intramural Research Program, National Institutes of Health, Baltimore, USA

[3]Dipartimento di Neuroscienze, Psicologia, Area del Farmaco e Salute del Bambino (NEUROFARBA), Sezione di Farmacologia e Tossicologia, Università degli Studi di Firenze, Firenze, Italy

[4]Dipartimento di Scienze Farmaceutiche, Università degli Studi di Milano, Milano, Italy

[5]Dipartimento di Fisica, Università di Cagliari, Cittadella Universitaria di Monserrato, Monserrato, Italy

Correspondence
Alessandro Piergentili and Wilma Quaglia, Scuola di Scienze del Farmaco e dei Prodotti della Salute, Università degli Studi di Camerino, Via Madonna delle Carceri, 62032 Camerino, Italy.
Email: alessandro.piergentili@unicam.it and wilma.quaglia@unicam.it

Funding information
Unione Europea-Next generation EU, "MUR fondo promozione e sviluppo, Grant/Award Number: DM737/2001; University of Camerino, Grant/Award Number: FAR 2022; the National Institute on Drug Abuse, Intramural Research Program

Abstract

A new series of muscarinic acetylcholine receptor (mAChR) ligands obtained by inserting different substituents in position 2 of the potent 6,6-diphenyl-1,4-dioxane antagonists **4** and **5** was designed and synthesized to investigate the influence of steric bulk on the mAChR affinity. Specifically, the insertion of a 2-methyl group, affording compounds **6** and **9**, resulted as the most favorable modification in terms of affinity for all muscarinic subtypes. As supported by computational studies performed on the hM_1 receptor, this substituent may contribute to stabilize the ligand within the binding site by favoring the formation of stable interactions between the cationic head of the ligand and the residue D105. The increase of steric bulk, obtained by replacing the methyl group with an ethyl (**7** and **10**) and especially a phenyl substituent (**8** and **11**), caused a marked decrease of mAChR affinity, demonstrating the crucial role played by the steric bulk of the 2-substituent in the mAChR interaction. The most intriguing result was obtained with the tertiary amine **9**, which, surprisingly, showed two different pK_i values for all mAChRs, with preferential subpicomolar affinities for the M_1, M_3, and M_4 subtypes. Interestingly, biphasic curves were also observed with both the eutomer (*S*)-(−)-**9** and the distomer (*R*)-(+)-**9**.

KEYWORDS
6,6-diphenyl-1,4-dioxane derivatives, biphasic curves in binding assays, computational studies, muscarinic receptor ligands, subpicomolar mAChR affinity

1 | INTRODUCTION

Muscarinic acetylcholine receptors (mAChRs) are a family of class A G protein-coupled receptors (GPCRs) consisting of five highly conserved subtypes, namely M_1, M_2, M_3, M_4, and M_5, with different molecular and signaling properties. M_1, M_3, and M_5 receptors have been shown to typically couple to G proteins of the $G\alpha_{q/11}$ family, causing the downstream activation of phospholipase Cβ and phosphatidylinositol (3,4,5)-trisphosphate turnover and the subsequent increase of cytosolic Ca^{2+}, as well as the stimulation of protein kinase C. The remaining M_2 and M_4 receptors predominantly couple to $G\alpha_{i/o}$ proteins to inhibit adenylyl cyclase, resulting in decreased levels of intracellular cyclic adenosine monophosphate levels.[1] The activation of mAChRs can transduce to a change in the activity of endogenous ion channels that regulate excitability: activation of βγ subunits of the $G_{i/o}$ proteins through M_2 and M_4 receptor stimulation modulates various ion channels including voltage-gated calcium channels[2] as well as G-protein coupled inwardly rectifying potassium channels (GIRK).[3]

Drugs targeting mAChRs are generally developed for the treatment of various diseases. Peripheral mAChRs are involved in widespread disorders such as overactive bladder (OAB) syndrome, where antagonists exert their effects by inhibiting the binding of acetylcholine at M_2 and M_3 mAChRs on detrusor smooth muscle cells,[4] or chronic obstructive pulmonary diseases (COPD), where long-acting mAChR antagonists show clinically meaningful effects in lung function,[5] and asthma.[6] Central mAChRs are important drug targets for the treatment of schizophrenia,[7,8] Alzheimer's disease,[9] Parkinson's disease[8], and drug addiction.[8] Furthermore, mAChRs have been demonstrated to be involved in other disorders like cancer,[10] diabetes,[11] cardiovascular diseases,[12] pain,[13] and inflammation.[14]

Saturated heterocycles are common elements in medicinal chemistry, with nitrogen heterocycles being ubiquitous and oxygen heterocycles such as oxetanes and tetrahydropyrans finding growing utility.[15–17] Heterocyclic compounds targeting mAChRs are numerous: among them, muscarine (**1**), an oxygen heterocycle derivative, is the specific natural agonist from which the mAChRs have derived their denomination, while atropine (**2**), possessing a nitrogen heterocyclic nucleus, is the typical antagonist (Figure 1).[18] The cationic nature of muscarine limits its diffusion through lipophilic barriers. Therefore, ingested or injected muscarine mainly targets peripheral mAChRs, while atropine, being a tertiary amine, indiscriminately blocks the mAChRs of both peripheral and central nervous systems.

Though the oxygen-containing heterocycle 1,4-dioxane has little been used in drug design, we have widely demonstrated that it is a bioversatile scaffold for the development of compounds interacting with different receptor systems,[19–27] including mAChRs.[28–33] Concerning this system, we have demonstrated that it is possible to obtain mAChR agonists or antagonists, depending on the kind of substituent in position 6 of the 1,4-dioxane nucleus, analogously to what had previously been observed for mAChR ligands bearing the 2-substituted 1,3-dioxolane ring.[34,35] Specifically, the presence of a 6-methyl group led to the potent muscarinic agonist **3**,[28–30] while its replacement with bulkier substituents allowed us to obtain potent antagonists,[31–33] including the quaternary ammonium 6,6-diphenyl derivative **4**.[31] Ligands bearing a tertiary amine, such as **5** (Figure 1), also proved to act as antagonists at mAChR,[31] probably by binding in the cationic form. The permanent positive charge in **4** might limit its ability to cross the blood–brain barrier (BBB), making it an interesting compound able to selectively block peripheral mAChRs, while the tertiary amine **5** might interact with both central and peripheral mAChRs. We also demonstrated that chirality plays a pivotal role in the interaction of 1,4-dioxane ligands with mAChRs, with the eutomer being the (*S*)-enantiomer for both compounds **4** and **5**.[31]

In this study, we designed and synthesized the quaternary ammonium compounds **6–8** and the tertiary amines **9–11** by inserting in position 2 of the potent 6,6-diphenyl-1,4-dioxane mAChR antagonists **4** and **5**, respectively, substituents of different size, namely a methyl (molar refractivity (MR) = 6.88 cm^3/mol), an ethyl (MR = 11.48 cm^3/mol), or a phenyl group (MR = 25.28 cm^3/mol), with the aim of evaluating the influence of the steric bulk on the mAChR affinity (Figure 2). The introduction of a phenyl ring would also allow us to value whether π-stacking interactions with aromatic amino acid residues in the binding site might contribute to the ligand–receptor interaction. Furthermore, considering the critical role played by chirality in the mAChR affinity of 1,4-dioxanes, the enantiomers (*R*)-(+)-**9** and (*S*)-(−)-**9** (Figure 2) were also prepared and studied.

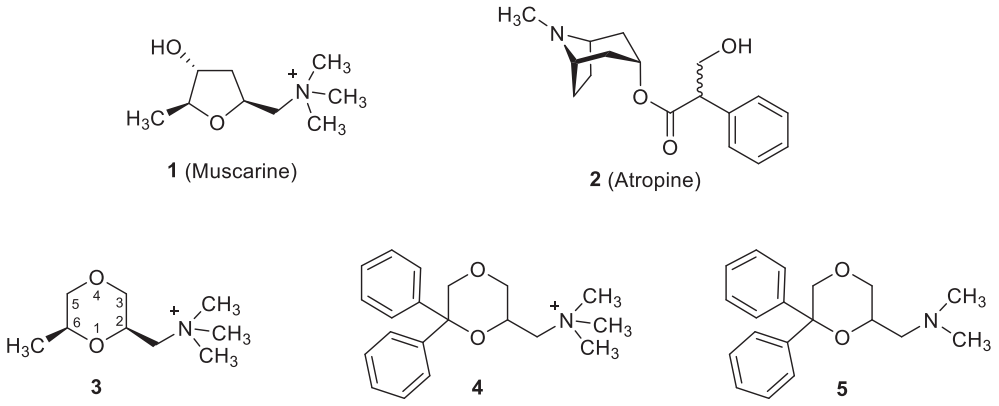

FIGURE 1 Structures of muscarine (**1**), atropine (**2**), and the 1,4-dioxane compounds **3–5**.

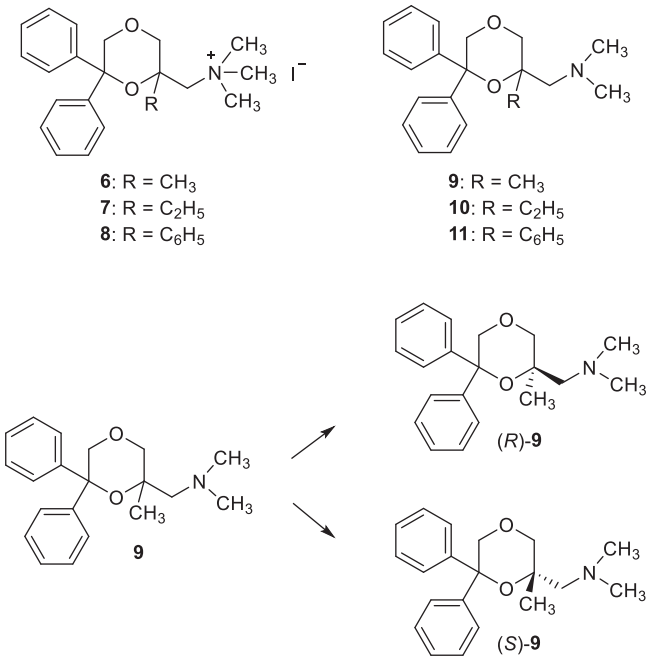

FIGURE 2 Structures of the novel compounds **6**–**11** and the enantiomers (*R*)-**9** and (*S*)-**9**.

2 | RESULTS AND DISCUSSION

2.1 | Chemistry

The synthesis of the new 1,4-dioxane compounds **6**–**11** is described in Scheme 1. The reduction of 2-ethylacrolein with $LiAlH_4$ yielded 2-methylenebutan-1-ol (**12**),[36] while 2-phenylprop-2-en-1-ol (**13**) was obtained by reacting prop-2-in-1-ol with phenyl magnesium bromide in the presence of CuI.[37] Alcohols **12** and **13** were condensed with ethyl 2-bromoacetate in the presence of NaH in tetrahydrofuran (THF), affording compounds **14** and **15**, respectively, whose reaction with phenyl lithium in diethyl ether led to the desired intermediates **16** and **17**. Alkenes **16** and **17** were subjected to epoxidation with *m*-chloroperoxybenzoic acid (*m*-CPBA), affording **18** and **19**, followed by treatment with (1*S*)-(+)−10-camphorsulfonic acid [(1*S*)-(+)-10-CSA] to give the 1,4-dioxanes **21** and **22**. The treatment of **20**,[32] **21**, and **22** with *p*-tosyl chloride yielded intermediates **23**–**25**, respectively, whose subsequent amination with dimethylamine afforded the desired tertiary amines **9**–**11**, which were transformed into the corresponding oxalate salts. The treatment of amines **9**–**11** with methyl iodide gave the methiodides **6**–**8**.

The enantiomers (+)-**9** and (−)-**9** were separated by preparative chiral HPLC (Supporting Information S2: Figure S1) and the enantiomeric excess (e.e.), determined by analytical high-performance liquid chromatography (HPLC), proved to be >98.5% for both enantiomers (Supporting Information S2: Figure S2).

To determine the absolute configuration of the 2-stereocenter, the two enantiomers were also prepared following the procedure reported in Scheme 2. The conversion of the 2-methyl-6,6-diphenyl-1,4-dioxane-2-carboxylic acid into the corresponding acyl chloride, followed by treatment with the lithium salt of the (*R*)-4-benzyl-2-oxazolidinone yielded the diastereomers (*R*,*R*)-**26** and (*S*,*R*)-**26**, which were separated by flash chromatography.[32] Their absolute configuration was assigned by X-ray diffraction analysis performed on the ester (*S*)-quinuclidin-3-yl (*S*)-2-methyl-6,6-diphenyl-1,4-dioxane-2-carboxylate, prepared starting from (*S*,*R*)-**26**, as previously reported.[32] Hydrolysis with simultaneous reduction of (*R*,*R*)-**26** and (*S*,*R*)-**26** with lithium borohydride in the presence of water provided the enantiomeric alcohol (*S*)-**20** and (*R*)-**20**, respectively, whose treatment with *p*-tosyl chloride afforded the corresponding intermediates (*R*)-**23** and (*S*)-**23**. Subsequent amination of the tosyl derivatives with dimethylamine gave the desired enantiomers (*S*)-(−)-**9** and (*R*)-(+)-**9**, respectively.

The *S* and *R* absolute configuration of (−)-**9** and (+)-**9** separated by preparative HPLC was assigned by comparing the sign of their optical rotations with those of (*S*)-(−)-**9** and (*R*)-(+)-**9** obtained by synthesis.

2.2 | Binding studies

The muscarinic pharmacological profiles of the novel compounds **6**–**11** were evaluated by receptor binding assays with human recombinant hM_1–hM_5 receptor subtypes stably expressed in Chinese hamster ovary (CHO-K1) cell lines by displacement of the labeled antagonist [^{3}H]*N*-methylscopolamine ([^{3}H]NMS). The affinity values, expressed as pK_i, are reported in Table 1 and Supporting Information S2: Figure S3 and compared with those of methiodide **4** and tertiary amine **5**.[31]

The analysis of the results reveals that, interestingly, the insertion of a methyl group in position 2 of the 1,4-dioxane nucleus of the methiodide **4**, affording compound **6**, caused a marked increase in affinity for all the five mAChR subtypes. The replacement of the methyl group with bulkier substituents proved to be less favorable for mAChR interaction. In particular, the 2-ethyl substituted derivative **7** showed hM_1–hM_5 affinity values significantly lower than those of **6**, even though its mAChR profile remains noteworthy, being superimposable to that of the potent antagonist **4**. A further increase of the steric bulk in position 2 strongly decreased the affinity for all mAChR subtypes, the 2-phenyl derivative **8** showing negligible hM_1–hM_5 affinity and, thus, representing the least active compound among the quaternary ammonium salts.

A similar SAR trend was detected for the tertiary amines **9**–**11**, for which a decrease of mAChR affinity was observed by replacing the methyl with an ethyl and especially a phenyl group, confirming that the steric bulk of the 2-substituent plays a crucial role in the mAChR interaction. For this set of compounds, not only the 2-methyl derivative **9** but also the 2-ethyl analog **10** showed affinity values higher than those of the unsubstituted lead compound **5**.

However, the most intriguing result was obtained with the 2-methyl compound **9** which, surprisingly, in the equilibrium binding assays showed two individual values of pK_i (high and low) (Figure 3) in all five mAChR subtypes, with a preferential affinity for M_1, M_3 and M_4 subtypes with respect to M_2 and M_5. Indeed, the higher

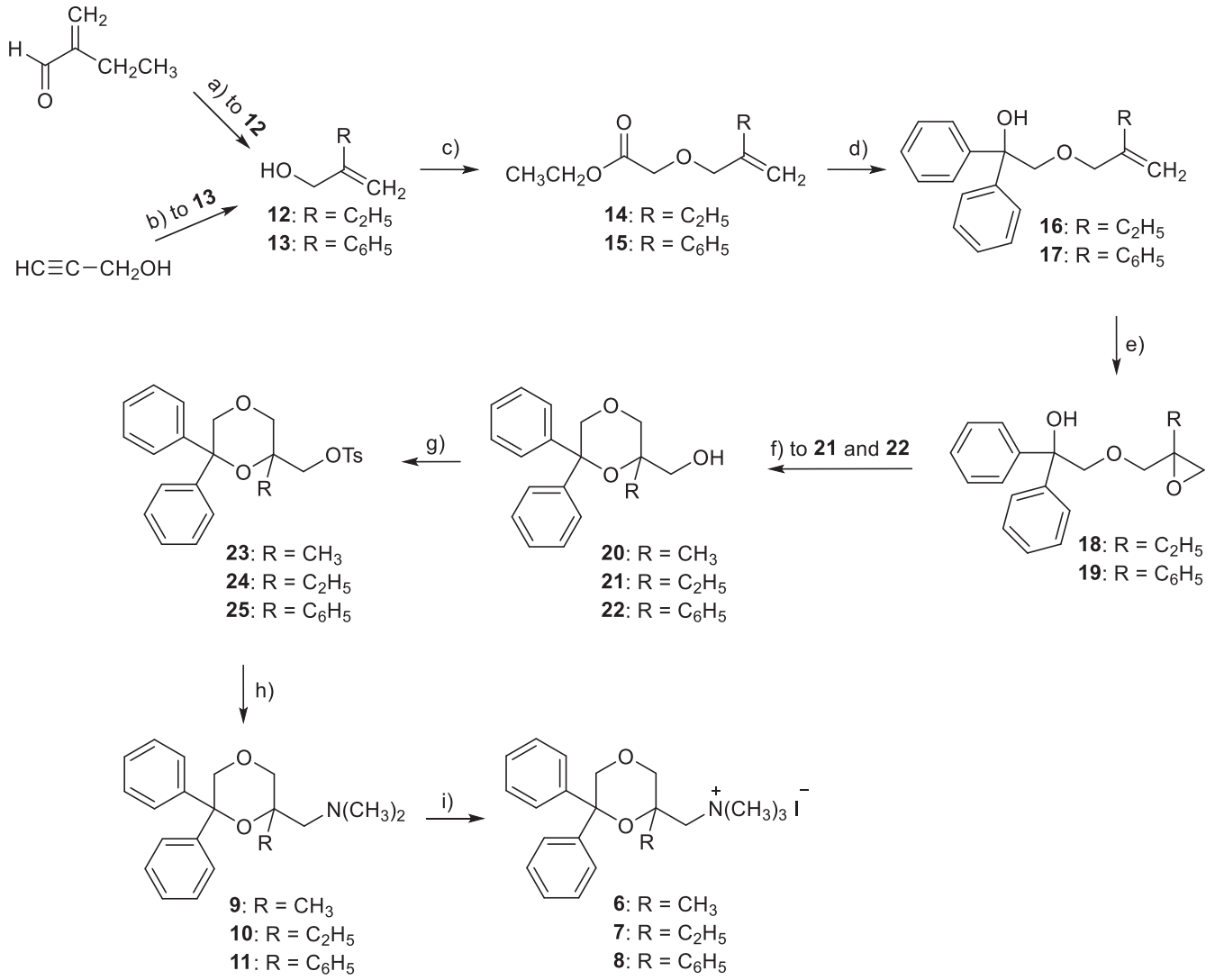

SCHEME 1 Reagents and conditions: (a) $LiAlH_4$, diethyl ether; (b) PhMgBr, CuI, diethyl ether; (c) ethyl 2-bromoacetate, NaH, THF (tetrahydrofuran); (d) PhLi, diethyl ether; (e) *m*-CPBA, CH_2Cl_2; (f) (1*S*)-(+)-10-CSA, CH_2Cl_2; (g) p-TsCl, pyridine; (h) $(CH_3)_2NH$, benzene; (i) CH_3I, diethyl ether.

R-squared (R^2) values obtained by processing the binding data with two-site models with respect to the one-site models demonstrate that the two-site model fits better on the data (see Supporting Information S2: Table S1).

A high-affinity binding was observed at pK_i values ranging from 9.11 to 14.08, with a high-affinity population of 32%–78%, while the pK_i for the low-affinity site ranged from 4.73 to 10.01 (Table 1). This experimental observation is hard to interpret, considering that the compounds of this series should bind the mAChR orthosteric site, analogously to our previously described 1,4-dioxane ligands.[33] Indeed, compounds showing biphasic curves in competition binding assays at mAChRs expressed in CHO-K1 cells using the radioligand [^{3}H]NMS are reported in the literature, but they are allosteric ligands such as gallamine or alkane-bis-ammonium compounds.[38] To our knowledge, no mAChR orthosteric ligands showing a biphasic curve have been described so far, and this might be associated with cross-modulation/crosstalk, or different binding stages, with mAChRs forming homodimers/oligomers within the expressing cells,[39] promoting these compounds as unique fascinating molecules to further investigate this aspect in future biomolecular assays. Indeed, GPCRs can be found in the plasma membrane as dimers and the biphasic competitive binding experiments could be caused by the presence of homodimers. Specifically, regarding mAChR subtypes, it has been reported that M_1,[40] M_2,[41] and M_3[42] can form homodimer and the biphasic curve could be due to the interaction of the ligand with the binding site of the monomer and the dimer, or between the two orthosteric sites of the dimeric form.

In M_1, M_3, and M_4 mAChR subtypes the high-affinity binding of compound **9** was observed at subpicomolar concentrations (pK_i = 13.57, 13.63, and 14.08, respectively), with receptor sites representing about 50% of the population, while in M_2 and M_5 subtypes at much higher concentrations, and with two different

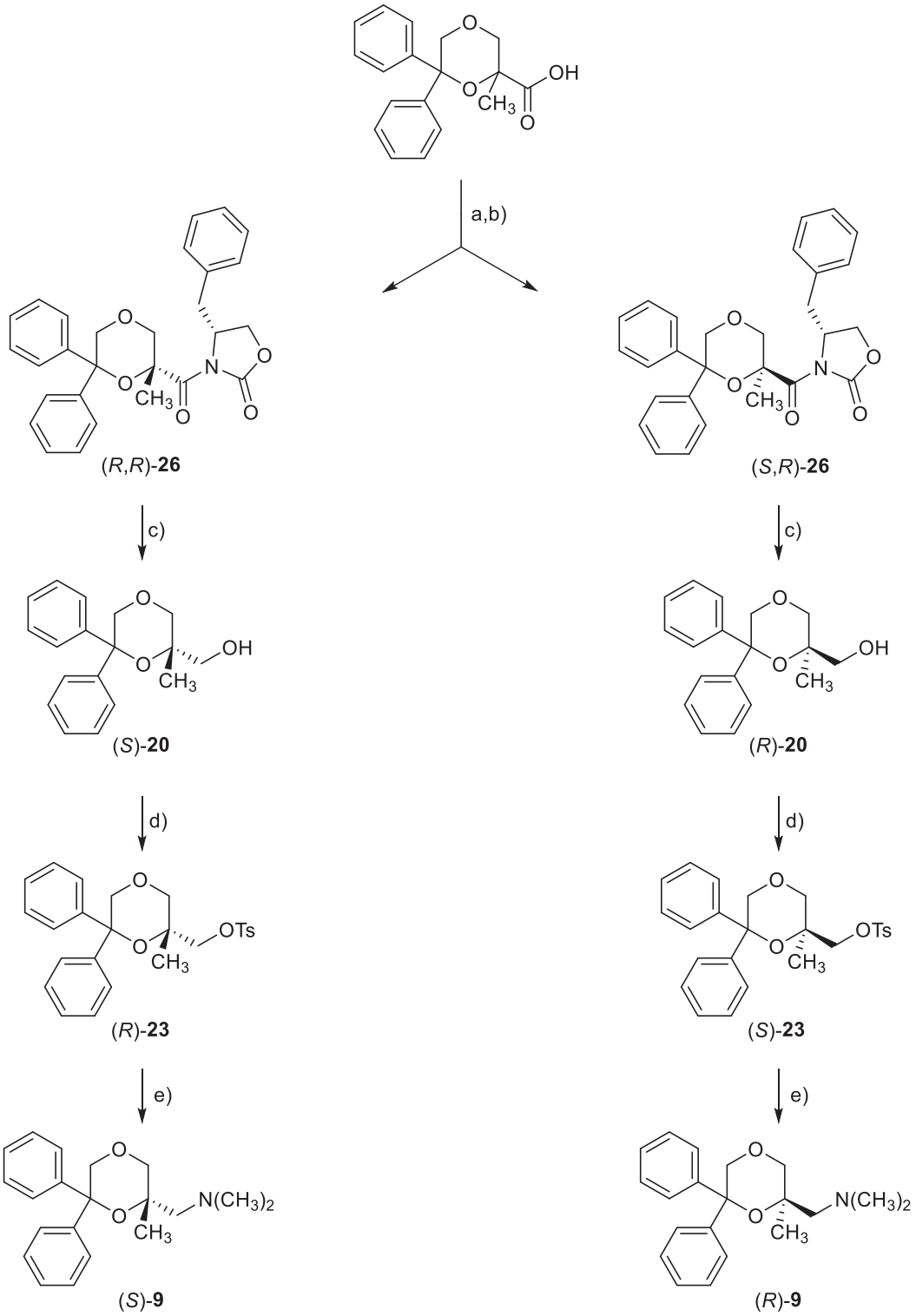

SCHEME 2 Reagents and conditions: (a) $(COCl)_2$, CH_2Cl_2, dimethylformamide (DMF); (b) *n*-BuLi, (*R*)-4-benzyl-2-oxazolidinone, THF (tetrahydrofuran), −78°C; (c) $LiBH_4$, diethyl ether, H_2O; (d) *p*-TsCl, pyridine; (e) $(CH_3)_2NH$, benzene.

levels of population (78% and 32% of high affinity site for M_2 and M_5, respectively).

The surprising profile of (±)-**9** prompted us to prepare and study its two enantiomers (*S*)-(−)-**9** and (*R*)-(+)-**9**, whose affinity values at human recombinant hM_1-hM_5 subtypes, expressed as pK_i, are shown in Table 2 and Supporting Information S2: Figure S4 in comparison with those of the lead **5** and its enantiomers (*S*)-(−)-**5** and (*R*)-(+)-**5**.[31]

The *S*-enantiomer of compound **9** represents the eutomer, with affinity values significantly higher than those of the distomer (*R*)-(+)-**9** toward all hM_1–hM_5 subtypes, analogously to what had previously

TABLE 1 Equilibrium binding affinity of compounds **4–11**.

Compd		pK_i[a] hM$_1$	hM$_2$	hM$_3$	hM$_4$	hM$_5$
(±)-**4**	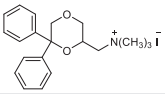	9.10 ± 0.08	8.24 ± 0.12	8.44 ± 0.10	8.58 ± 0.06	8.36 ± 0.09
(±)-**5**	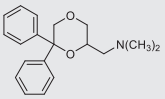	8.34 ± 0.10	7.78 ± 0.09	8.66 ± 0.13	8.31 ± 0.04	8.27 ± 0.11
(±)-**6**	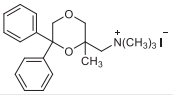	10.93 ± 0.06	10.64 ± 0.05	9.99 ± 0.11	10.58 ± 0.06	10.20 ± 0.06
(±)-**7**	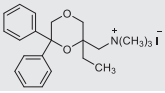	9.02 ± 0.04	8.43 ± 0.06	8.44 ± 0.03	8.48 ± 0.03	8.20 ± 0.03
(±)-**8**	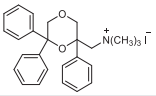	7.05 ± 0.07	5.82 ± 0.07	6.14 ± 0.04	6.09 ± 0.04	5.82 ± 0.05
(±)-**9**	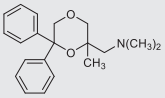	13.57 ± 0.30 (high) 57 ± 5%[b] 9.85 ± 0.27(low)	9.11 ± 0.35 (high) 78 ± 6%[b] 4.73 ± 0.73 (low)	13.63 ± 0.25 (high) 48 ± 4%[b] 9.74 ± 0.15 (low)	14.08 ± 0.47 (high) 40 ± 5%[b] 10.01 ± 0.15 (low)	10.51 ± 0.42 (high) 32 ± 4%[b] 7.58 ± 0.19 (low)
(±)-**10**	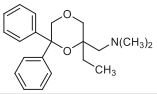	9.32 ± 0.05	8.93 ± 0.08	8.81 ± 0.05	8.83 ± 0.06	8.50 ± 0.04
(±)-**11**	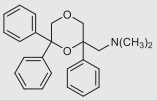	6.60 ± 0.06	6.58 ± 0.13	5.99 ± 0.07	5.92 ± 0.08	5.74 ± 0.09

[a]Inhibition binding constants (pK_i) of the compounds for human cloned muscarinic receptors expressed in CHO-K1 cells. The values represent the arithmetic mean ± S.E.M. of 4–8 experiments performed in duplicate. A model involving two classes of sites was significantly better than a model involving a single class of sites in all cases (hM$_1$, hM$_3$, hM$_4$, hM$_5$ $p < 0.005$; hM$_2$, $p < 0.01$). High, negative logarithm of the dissociation constant for the high-affinity binding site. Low, negative logarithm of the dissociation constant for the low-affinity binding site.

[b]Fraction representing the high-affinity binding site in %.

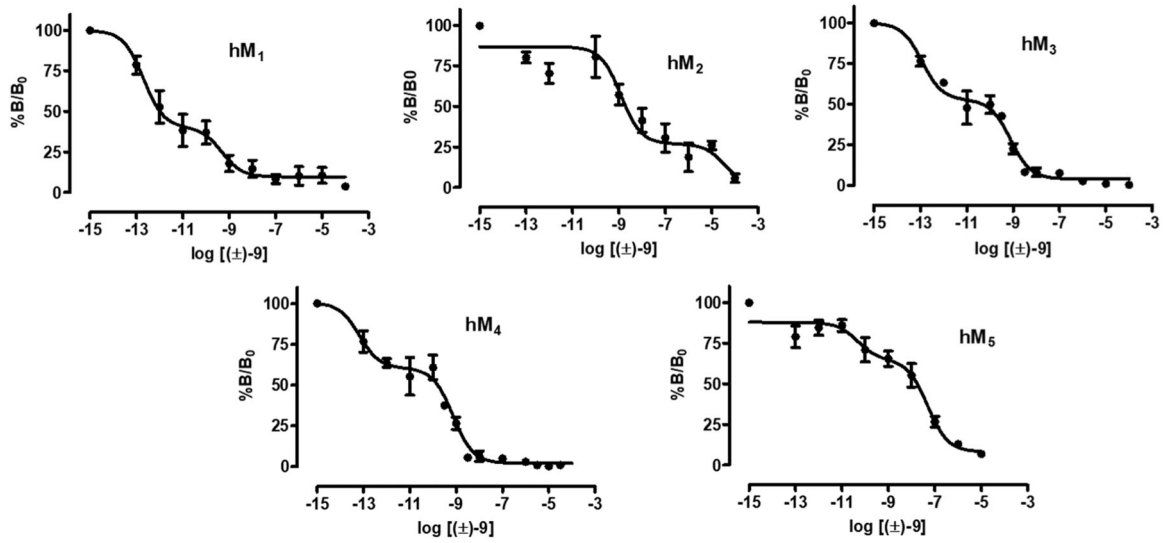

FIGURE 3 Inhibition of specific binding of 0.2 nM [^{3}H] NMS by (±)-**9** at the five human cloned muscarinic receptors. The curves show the predicted relationship for a two-site model. Points represent the mean ± S.E.M. of 4-8 experiments conducted in duplicate.

TABLE 2 Equilibrium binding affinity of compounds **5** and **9** and the enantiomers (*S*)-(−)-**5**, (*R*)-(+)-**5**, (*S*)-(−)-**9**, and (*R*)-(+)-**9**.

Compd		pK_i[a] hM_1	hM_2	hM_3	hM_4	hM_5
(±)-**5**	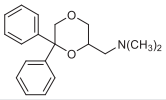	8.34 ± 0.10	7.78 ± 0.09	8.66 ± 0.13	8.31 ± 0.04	8.27 ± 0.11
(*S*)-(−)-**5**	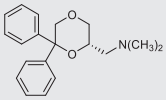	8.90 ± 0.15	8.01 ± 0.11	8.82 ± 0.09	8.63 ± 0.20	8.74 ± 0.12
(*R*)-(+)-**5**	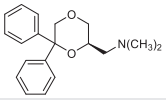	7.45 ± 0.06	7.02 ± 0.17	7.14 ± 0.13	7.15 ± 0.11	7.09 ± 0.18
(±)-**9**	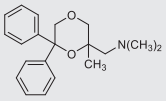	13.57 ± 0.30 (high) 57 ± 5%[b] 9.85 ± 0.27 (low)	9.11 ± 0.35 (high) 78 ± 6%[b] 4.73 ± 0.73 (low)	13.63 ± 0.25 (high) 48 ± 4%[b] 9.74 ± 0.15 (low)	14.08 ± 0.47 (high) 40 ± 5%[b] 10.01 ± 0.15 (low)	10.51 ± 0.42 (high) 32 ± 4%[b] 7.58 ± 0.19 (low)
(*S*)-(−)-**9**	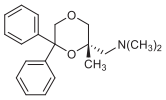	14.99 ± 0.15 (high) 60 ± 3%[b] 9.66 ± 0.19 (low)	10.70 ± 0.18 (high) 62 ± 5%[b] 7.00 ± 0.32 (low)	13.72 ± 0.22 (high) 34 ± 3%[b] 9.15 ± 0.11 (low)	14.51 ± 0.29 (high) 37 ± 4%[b] 9.10 ± 0.13 (low)	11.23 ± 0.50 (high) 29 ± 6%[b] 7.92 ± 0.18 (low)
(*R*)-(+)-**9**	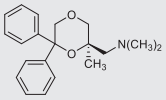	10.59 ± 0.25 (high) 26 ± 3%[b] 7.78 ± 0.08 (low)	7.12 ± 0.36 (high) 11 ± 3%[b] 5.88 ± 0.29 (low)	7.75 ± 0.12 (high) 77 ± 8%[b] 6.00 ± 0.38 (low)	7.23 ± 0.06	9.68 ± 0.38 (high) 26 ± 5%[b] 6.39 ± 0.12 (low)

[a]Inhibition binding constants (pK_i) of the compounds for human cloned muscarinic receptors expressed in CHO-K1 cells. The values represent the arithmetic mean ± S.E.M. of 4–8 experiments performed in duplicate. A model involving two classes of sites was significantly better than a model involving a single class of sites in all cases. High, negative logarithm of the dissociation constant for the high-affinity binding site. Low, negative logarithm of the dissociation constant for the low-affinity binding site

[b]Fraction representing the high-affinity binding site in %.

been observed for lead **5**, confirming that the *S* configuration of carbon in position 2 of the 1,4-dioxane nucleus is the preferred one for the interaction with the mAChR binding site. As observed with the racemic compound (±)-**9**, also in the case of the enantiomers (*S*)-(−)-**9** and (*R*)-(+)-**9** biphasic curves were detected in the displacement of the [^{3}H]NMS, with the exception of (*R*)-(+)-**9** at the M_4 subtype.

The binding profile of the eutomer (*S*)-(−)-**9** was similar to that of the racemic compound (±)-**9** with significantly higher affinities for M_1, M_3, and M_4 subtypes with respect to M_2 and M_5 subtypes. Instead, the distomer (*R*)-(+)-**9** possessed a different pharmacological profile, showing selectivity for M_1 and M_5 over M_2, M_3 and M_4 subtypes.

2.3 | Molecular modeling studies

The binding mode of both enantiomers of the lead compound **5**, of the most active derivative **9** and of its quaternary congener **6** was explored through a computational procedure involving docking and molecular dynamics (MD) simulations, by using the crystal structure of human M_1 receptor in complex with the antagonist tiotropium (PDB ID 5CXV).[43]

The docking outcomes highlighted that the cationic head of the analyzed derivatives could engage the conserved D105(TM3) and W378(TM6) to form a salt bridge and a π–cation interaction, respectively (Figure 4). In addition, the positively charged group of (*S*)-(−)-**9**, (*R*)-(+)-**9**, and (*R*)-(+)-**5** might be involved in H-bonds with S109(TM3). This was not observed for the *S*-enantiomer of compound **5** whose distance between the hydrogen of the protonated tertiary amine and the oxygen of S109(TM3) side chain is equal to 3.95 Å. Hydrophobic contacts involving the phenyl rings and the residues Y106(TM3), W378(TM6), W157(TM4), A193(TM5), and A196(TM5) were detected for all the studied molecules. In the *S*-enantiomers of derivatives **5** and **9** (Figure 4a,c) and in both stereoisomers of compound **6** (Figure 4e,f) one of the two aromatic rings is involved in π-stacking interactions with W378(TM6), while the same contact is established with W157(TM4) in the case of the *R*-enantiomers of **5** and **9** (Figure 4b,d). Moreover, the eutomers (*S*)-(−)-**5** (Figure 4a) and (S)-(−)-**9** (Figure 4c) might also elicit additional hydrophobic contacts with V113(TM3) and L183 which might contribute to their higher affinity toward hM_1 if compared with the corresponding *R*-enantiomers. Hydrophobic interactions with V113 were also detected for both stereoisomers of compound **6**. In addition, the *S*-enantiomer of **6** could also form an H-bond with Y106(TM3) through one of the oxygen atoms of the dioxane ring. Regarding the most active derivative **9**, the methyl group is seen in proximity of Y106(TM3) and W157(TM4) in the docking pose of the distomer (*R*)-(+)-**9** (Figure 4d), while it occupies a lipophilic pocket lined by W387(TM6), Y381(TM6), Y404(TM7), and C407(TM7)

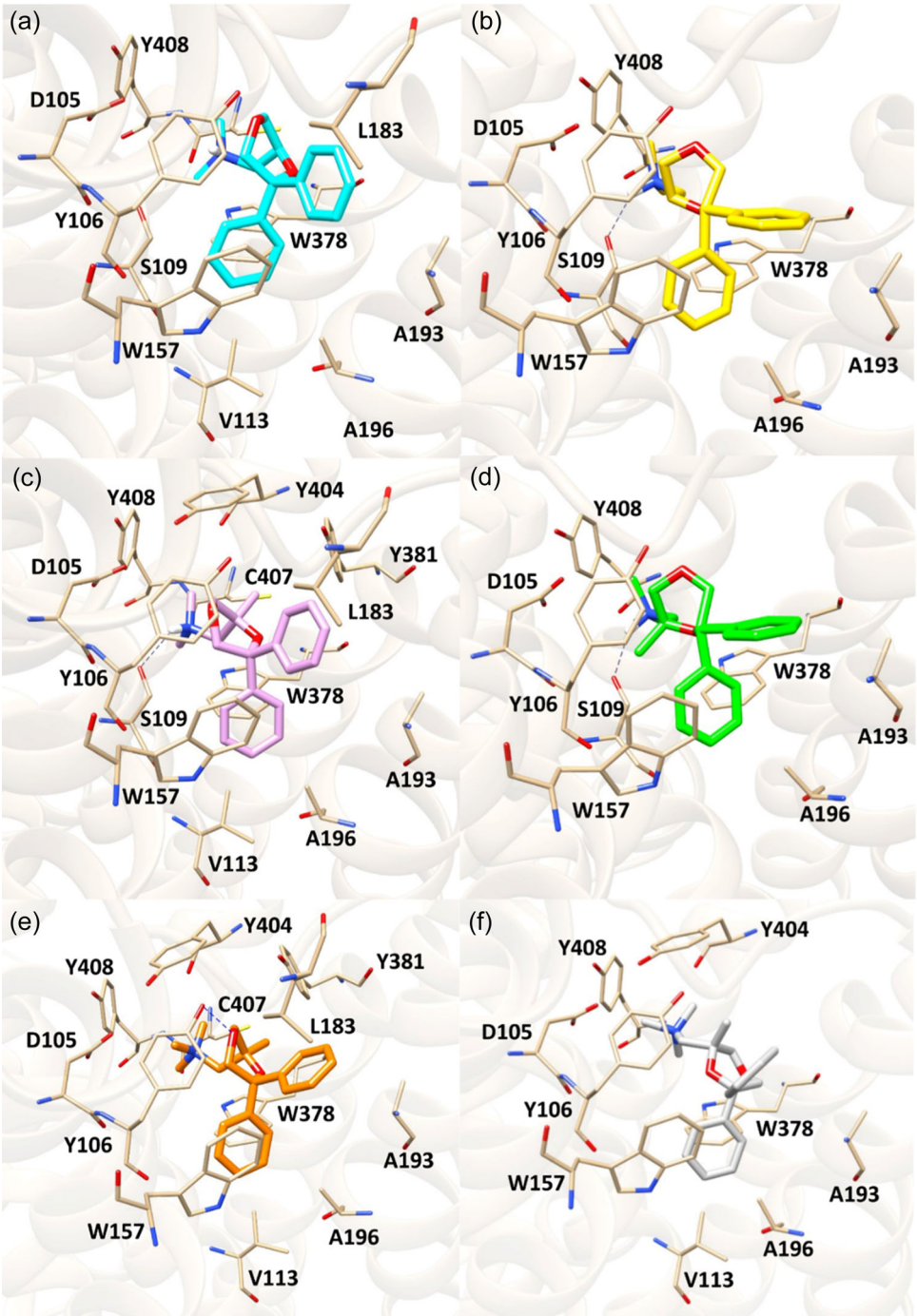

FIGURE 4 Docking poses of compounds (a) (*S*)-(−)-**5** (cyan sticks), (b) (*R*)-(+)-**5** (yellow sticks), (c) (*S*)-(−)-**9** (pink sticks), (d) (*R*)-(+)-**9** (green sticks), (e) (*S*)-(−)-**6** (orange sticks), and (f) (*R*)-(+)-**6** (gray sticks) within hM_1 binding site. H-bonds are depicted as blue dashed lines.

in the binding pose of the eutomer (*S*)-(−)-**9** (Figure 4c) enabling the formation of further hydrophobic contacts. A similar orientation was observed for the *S*-enantiomer of its quaternary analog **6** (Figure 4e), while in the pose of (*R*)-(+)-**6** (Figure 4f) the methyl group faces the opposite side with respect to (*R*)-(+)-**9** and does not elicit any significant interaction with the residues of the binding pocket.

To get more insights about the enantioselectivity and different activity profiles observed for derivatives **5**, **6**, and **9**, the docking poses described above were subjected to 300 ns MD simulations. Indeed, MD is widely used as post-processing tool as it allows exploring the flexibility of both protein and ligand which strongly influences the binding process.[44] The stability of the simulated complexes was monitored by root-mean square deviation (RMSD) analysis as depicted in Figure 5. After some initial fluctuations, the most potent derivative (*S*)-(−)-**9** (Figure 5a) assumed a very stable behavior during the trajectory with an average RMSD value of 0.30 Å.

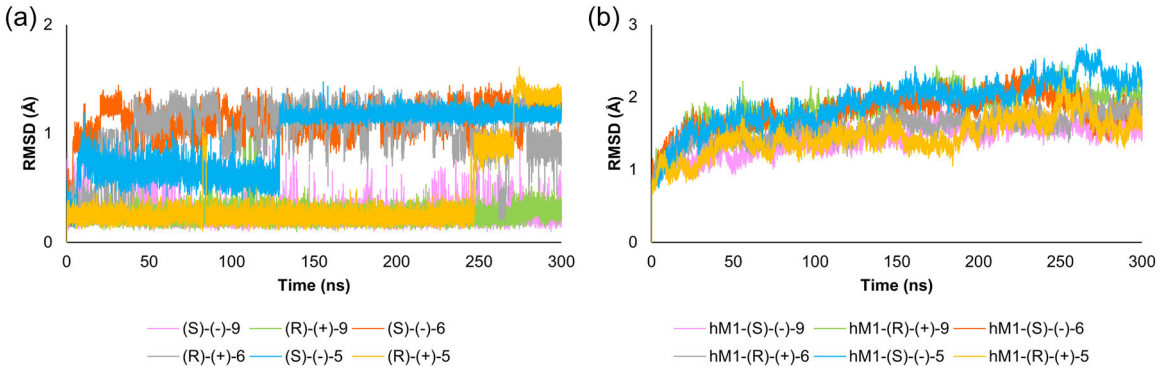

FIGURE 5 (a) Root-mean square deviation (RMSD) profiles of both enantiomers of compounds **5**, **6** and **9**. (b) RMSD plot of the backbone of hM_1 receptor in complex with the analyzed inhibitors.

A similar profile was observed for its enantiomer (*R*)-(+)-**9** characterized by a mean RMSD of 0.26 Å. In contrast, a greater mobility into hM_1 binding site was detected for both enantiomers of compounds **5** and **6**. More specifically, the RMSD values of the eutomer (*S*)-(−)-**5** increased at the beginning of the simulation, reaching values around 0.7 Å and then at about 130 ns assuming values of about 1.2 Å, remaining stable for the rest of the simulation time. Concerning the distomer (*R*)-(+)-**5**, its RMSD profile was similar to those observed for both enantiomers of compound **9** until 250 ns, after which the RMSD increased adopting values around 1.4 Å. Similar RMSD profiles were obtained for both enantiomers of compound **6** which showed an increment of the RMSD values at the beginning of the simulation, reaching values of around 1 Å, and several fluctuations throughout the trajectory. Regarding the RMSD analysis of the hM_1 backbone (Figure 5b), a higher mobility was detected in all the simulated systems if compared with the respective ligands. Interestingly, in the complex involving the eutomer (*S*)-(−)-**9**, the protein showed the most stable profile with slighter fluctuations in respect to the other systems.

Cluster analysis enabled the exploration of the different conformations adopted by the ligands during the simulation. In addition, interaction fingerprints were computed to quantitatively characterize the protein–ligand interactions throughout the trajectory (Supporting Information S2: Figure S5). As expected, only one cluster was obtained for both enantiomers of derivative **9** whose representative structures are depicted in Figure 6. In both cases, the hydrogen of the protonated tertiary amine shifts toward D105(TM3) establishing an H-bond that is maintained throughout all the simulation time along with the salt bridge also detected in the respective docking poses. In the trajectory involving the eutomer (*S*)-(−)-**9**, the methyl group moves toward Y106(TM3) and D105(TM3) forming persistent hydrophobic contacts (100% and 73%, respectively), while in the distomer (*R*)-(+)-**9** the methyl group engages in hydrophobic interactions with W378(TM6) and C407(TM7) (100% and 87% persistence, respectively). Aromatic interactions were observed between (i) (*S*)-(−)-**9** and Y381(TM6) (61% persistence) and (ii) (*R*)-(+)-**9** and Y106(TM3) (47% persistence). Moreover, both enantiomers were able to form stable hydrophobic contacts with T189(TM5), Y381(TM6), and Y404(TM7) which is also implicated in π−cation interactions with (*R*)-(+)-**9**. Additional hydrophobic interactions were detected between the aromatic rings of i) derivative (*R*)-(+)-**9** and Y106(TM3) (100%), F197(TM5) (92%), L183 (85%) and N382(TM6) (31%), and ii) its enantiomer (*S*)-(−)-**9** and W378(TM6) (100%), C407(TM7) (100%), T192(TM5) (95%), A193(TM5) (69%), A196(TM5) (54%), and Y179(TM5) (41%). Overall, the interaction fingerprints analysis (Supporting Information S2: Figure S5A) revealed that the eutomer (*S*)-(−)-**9** was able to form more stable hydrophobic contacts with the surrounding residues compared with the distomer (*R*)-(+)-**9** (Supporting Information S2: Figure S5B), which might contribute to its higher affinity for hM_1 receptor.

Concerning compound **6**, four and three clusters were obtained from the MD simulations of the *S*- and the *R*-enantiomer, respectively. The most persistent conformations of the two stereoisomers (Figure 7) appeared in both cases for 37% of the simulation time. The analysis of the ligand–protein interaction fingerprints (Figure S5C,D) revealed that the quaternization of the tertiary amino group, with the consequent inability to form H-bonds, leads to a less stable interaction with D105(TM3). Indeed, the salt bridge with the side chain of D105(TM3) observed in the docking pose persists for 35% and 69% of the trajectory involving (*S*)-(−)-**6** and (*R*)-(+)-**6**, respectively. This finding might explain the less potency obtained for the racemic form of compound **6** if compared with **9**. In the *S*-enantiomer the cationic head appeared to be stabilized by stable π−cation interaction with Y408(TM7) (79%). The same interaction was retrieved for 40% of the simulation time between the *R*-enantiomer and Y404(TM7). Both stereoisomers were able to engage in stable hydrophobic contacts with Y404(TM7), Y106(TM3), Q110(TM3), W157(TM4), A196(TM5), W378(TM6), C407(TM7), and Y381(TM6). Additional hydrophobic interactions were observed between (*S*)-(−)-**6** and T192(TM5) (98%), V385(TM6) (77%) and V113(TM3) (38%). Instead, (*R*)-(+)-**6** was able to form further hydrophobic contacts with L183 (94%), T189(TM5) (87%), A193(TM5) (96%), and F197(TM5) (49%), a H-bond with N382(TM6) (91%) and a π-stacking interaction with Y106(TM3) (41%).

Concerning the lead compound **5**, two and three clusters were obtained for its *S*- and *R*-enantiomers, respectively. In more detail,

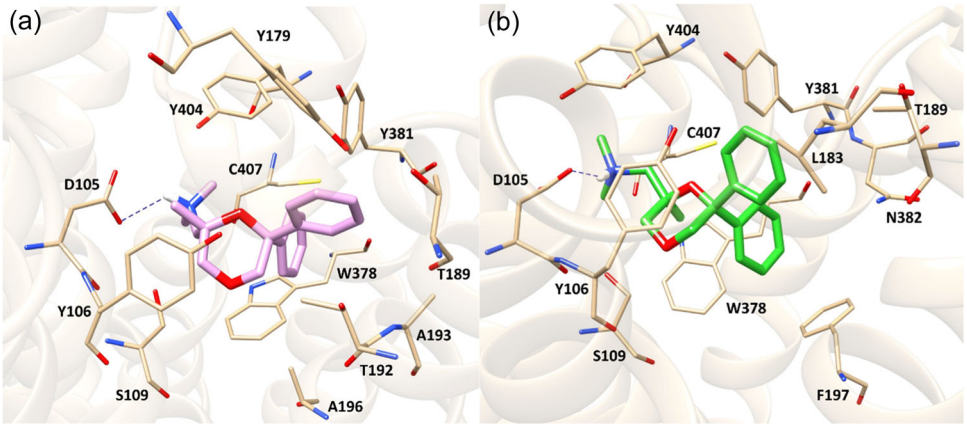

FIGURE 6 Representative conformations of (a) (*S*)-(−)-**9** and (b) (*R*)-(+)-**9** in complex with hM_1 receptor, obtained by cluster analysis. H-bonds are represented by blue dashed lines.

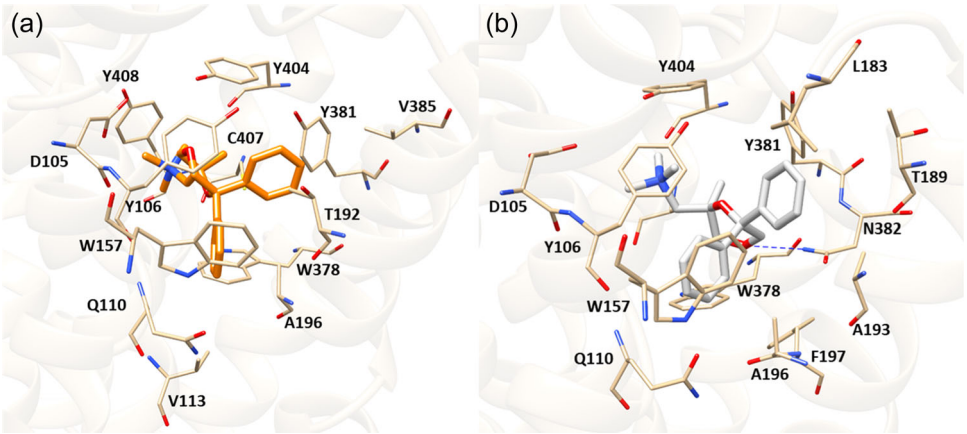

FIGURE 7 Representative conformations of (a) (*S*)-(−)-**6** and (b) (*R*)-(+)-**6** in complex with hM_1 receptor, obtained by cluster analysis. H-bonds are represented by blue dashed lines.

the most persistent conformer of (*S*)-(−)-**5** (Figure 8a) appears for 57% of the simulation time characterizing the second part of the trajectory, when the system converges (Figure 5a). During the MD simulation, the cationic head of (*S*)-(−)-**5** approaches S109(TM3) forming a stable H-bond, while preserving the salt bridge with D105(TM3) for about 75% of the simulation time (Supporting Information S2: Figure S5C). In addition, several hydrophobic contacts were detected between the phenyl rings of the inhibitor and Y106(TM3) (100%), A196(TM5) (100%), Q110(TM3) (100%), W378(TM6) (100%), A193(TM5) (51%), V113(TM3) (42%), W157(TM4) (93%), F197(TM5) (58%), Y381(TM6) (47%), and N382(TM6) (31%).

Regarding the *R*-enantiomer of lead **5**, its most prevalent conformer is present for 82% of the simulation time, from the beginning until ~250 ns, after which the RMSD values increase as described above (Figure 5a). To better understand the changes observed in the RMSD profile of (*R*)-(+)-**5**, the representative structure of the most populated cluster was superimposed to the second most frequent conformer (10% persistence), which characterizes the last part of the trajectory, as shown in Figure 8b. The most interesting shift concerns the protonated tertiary amine group of the molecule which points toward D105(TM3) in the most persistent conformer while facing the opposite side at the end of the simulation (Figure 8b). In addition, the average distance detected during the simulation between the cationic head of (*R*)-(+)-**5** and D105(TM3) is 5.44 Å, highlighting that the salt bridge observed in the initial docking pose does not persist during the simulation. Interaction fingerprints analysis (Supporting Information S2: Figure S5E) highlighted that the most stable interactions involve the residues W378(TM6) (99%), A196(TM5) (98%), A193(TM5) (71%), F197(TM5) (92%), W157(TM4) (85%), L183 (86%), V113(TM3) (89%), V385(TM6) (71%), Y106(TM3) (54%), and in less extent T189(TM5) (30%), which are all engaged in hydrophobic contacts with the ligand. Furthermore, a π−cation interaction between the protonated tertiary amine group and Y404(TM7) was detected for the 78% of the simulation time.

The outcomes of our computational study performed on hM_1 receptor pointed out that the presence of the methyl group not only allows additional contacts to be engaged, thus contributing to further stabilize the ligand within the binding site, but, along with the

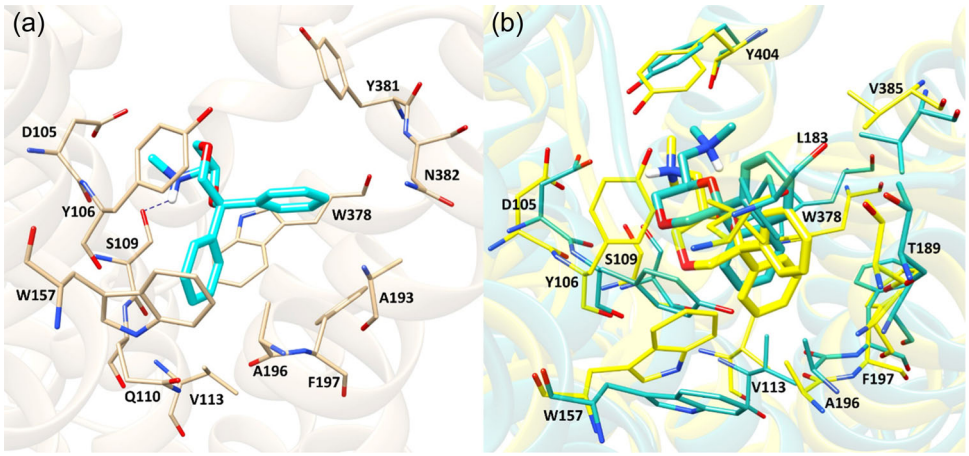

FIGURE 8 (a) Most prevalent conformer (57%) of (*S*)-(−)-**5** obtained by cluster analysis. (b) Most persistent conformations (82%) of (*R*)-(+)-**5** (yellow) superimposed to the representative structure of the last 10% of the MD simulation of hM_1-(*R*)-(+)-**5** complex (green).

protonated tertiary amine, also favors the formation of stable interactions between the cationic head of the ligands and the crucial residue D105(TM3). Indeed, the *R*-enantiomer of lead **5**, which lacks the methyl moiety, was not able to elicit persistent interactions with D105 during the MD simulation, while the *S*-enantiomer engages this residue for the 70% of the trajectory. Similar results were observed for derivative **6** bearing a quaternary ammonium group which is unable to establish H-bonds with D105(TM3), leading to less stable contacts with this residue. Furthermore, our results suggest that the *S*-enantiomers of **5** and **9** are able to form additional contacts if compared with the respective *R*-enantiomers, which might explain their higher potency.

To give a possible explanation to the biphasic binding curve observed for compound **9**, in silico studies including docking and MD simulations were performed to evaluate the capability of this derivative to bind the hM_1 allosteric pocket. The same analysis was conducted for the lead **5** for which a monophasic curve was obtained. The outcomes (data not shown) revealed no significant differences in the behavior of the two ligands when also bound to the allosteric site, thus suggesting that the biphasic curve obtained in the competition binding assay for derivative **9** could be related to the formation of homodimers/oligomers within the expressing cells or to cross-modulation/crosstalk mechanisms.[39]

3 | CONCLUSION

In this article, the influence on the mAChR affinity of substituents with different steric bulks in position 2 of the 1,4-dioxane nucleus of leads **4** and **5** has been investigated by the synthesis and study of the quaternary ammonium compounds **6**–**8** and the tertiary amines **9**–**11**. Specifically, the insertion of a methyl group, affording compounds **6** and **9**, proved to be the most favorable modification in terms of affinity for all muscarinic subtypes. Computational studies performed on hM_1 receptor supported this observation, highlighting that the presence of the methyl group contributes to stabilize the ligand within the binding site not only allowing additional contacts to be engaged, but also favoring the formation of stable interactions between the cationic head of the ligands and the crucial residue D105. A marked decrease of pK_i values was observed by replacing the methyl group with an ethyl (compounds **7** and **10**) and especially a phenyl substituent (compounds **8** and **11**), demonstrating the crucial role played by the 2-substituent in the mAChR interaction. The most fascinating result was obtained with the tertiary amine **9** which, surprisingly, showed two different pK_i values (high and low) for all five mAChRs, with preferential subpicomolar affinities for M_1, M_3, and M_4 subtypes. Interestingly, biphasic curves in the displacement of the [^{3}H]NMS were also observed with both the eutomer (*S*)-(−)-**9** and the distomer (*R*)-(+)-**9**. Considering that, to our knowledge, these are the first mAChR orthosteric ligands showing biphasic curves described so far, the 2-methyl derivative **9** and its eutomer (*S*)-(−)-**9** would deserve to be pharmacologically investigated in depth and they might become interesting tools to elucidate pharmacological properties of mAChRs homodimerization/oligomerization.

4 | EXPERIMENTAL

4.1 | Chemistry

4.1.1 | General

Melting points were taken in glass capillary tubes on a Büchi SMP-20 apparatus and are uncorrected. IR and NMR spectra were recorded on PerkinElmer 297 and Varian Mercury AS400 instruments, respectively. Chemical shifts are reported in parts per million (ppm) relative to tetramethylsilane (TMS), and spin multiplicities are given as s (singlet), d (doublet), dd (double doublet), t (triplet), or m (multiplet). IR spectral data (not shown because of the lack of unusual features) were obtained for all compounds reported and are consistent with the assigned structures. Mass spectra were obtained using a Hewlett

Packard 1100 MSD instrument utilizing electron-spray ionization (ESI). The microanalyses were recorded on FLASH 2000 instrument (ThermoFisher Scientific). Optical activity was measured at 20°C with a Perkin-Elmer 241 polarimeter. All reactions were monitored by thin-layer chromatography (TLC) using silica gel plates (60 F254; Merck), visualizing with ultraviolet light. Chromatographic separations were performed on silica gel columns (Kieselgel 40, 0.040–0.063 mm, Merck) by flash chromatography. Preparative chiral HPLC was performed using a Teledyne Isco EZ-Prep chromatography system with Diode Array Detector (DAD) and Evaporative Light Scattering detectors. HPLC analysis was performed using an AgilentTechnologies 1260 Infinity system coupled with DAD. For each analytical HPLC run multiple DAD λ absorbance signals were measured in the range of 230–280. Separation of the analyte, determination of purity, and relative excess of enantiomers were achieved at 40°C. Preparative and analytical HPLC columns were purchased from Daicel Corporation and Phenomenex. Optical rotations were determined using a Jasco DIP-370 polarimeter. Compounds were named following IUPAC rules as applied by ChemBioDraw Ultra (version 11.0) software for systematically naming organic chemicals. The purity of the novel compounds was determined by elemental analysis. MR values were calculated using the software ChemDraw Professional 23.0. The elemental composition of the compounds agreed to within ±0.4 percentage points of the calculated value. The ^{1}H-NMR spectra of the newly investigated compounds **6–11** are reported in the Supporting Information S2: Figures S6-S11.

The InChI codes of the investigated compounds, together with some biological activity data, are provided as Supporting Information S1.

4.1.2 | Synthesis of *N,N,N*-trimethyl-1-(2-methyl-6,6-diphenyl-1,4-dioxan-2-yl)methanaminium iodide (**6**)

A solution of **9** (4.0 mmol) in acetone (15 mL) was treated with an excess of methyl iodide. After 24 h at room temperature, the solid was filtered and recrystallized from 2-PrOH to give **6** in 68% yield (mp 219–220°C). ^{1}H NMR (DMSO-d6): δ 1.03 (s, 3H, CH_3), 3.25 (s, 9H, $N(CH_3)_3$), 3.25-4.01 (m, 5H, CH_2N, cycle), 4.82 (d, 1H, cycle), 7.21–7.37 (m, 10H, ArH). ^{13}C NMR (DMSO-d6): δ 22.2, 55.7, 67.9, 71.2, 71.5, 72.8, 75.6, 126.3, 127.2, 127.4, 128.0, 128.3, 130.0, 145.1, 145.8. ESI/MS (CH_3OH): m/z 326.3 $[M]^+$. Anal. calcd for $C_{21}H_{28}INO_2$: C 55.64, H 6.23, N 3.09, found: C 55.41, H 6.32, N 3.19.

4.1.3 | Synthesis of *N,N,N*-trimethyl-1-(2-ethyl-6,6-diphenyl-1,4-dioxan-2-yl)methanaminium iodide (**7**)

This compound was prepared starting from **10** following the procedure described for **6**. A solid was obtained which was recrystallized from EtOH (45% yield): mp 148–150°C. ^{1}H NMR (DMSO-d6): δ 0.61 (t, 3H, CH_3), 1.23–1.48 (m, 2H, CH_2), 3.24 (s, 9H, $N(CH_3)_3$), 3.26–3.64 (m, 4H, CH_2N, CH_2O), 3.79 (d, 1H, OCH_2), 4.91 (d, 1H, OCH_2), 7.18-7.52 (m, 10H, ArH). ^{13}C NMR (DMSO-d6): δ 9.1, 27.3, 55.8, 67.6, 69.7, 72.3, 77.3, 77.5, 126.2, 127.6, 127.8, 128.2, 128.6, 130.1, 144.9, 145.6. ESI/MS (CH_3OH): m/z 340.3 $[M]^+$. Anal. calcd for $C_{22}H_{30}INO_2$: C 56.54, H 6.47, N 3.00, found: C 56.22, H 6.65, N 2.92.

4.1.4 | Synthesis of *N,N,N*-trimethyl-1-(2,6,6-triphenyl-1,4-dioxan-2-yl)methanaminium iodide (**8**)

This compound was prepared starting from **11** following the procedure described for **6**. A solid was obtained which was recrystallized from EtOH (35% yield): mp 163–164°C. ^{1}H NMR (DMSO-d6): δ 2.80 (s, 9H, $N(CH_3)_3$), 3.80–4.19 (m, 4H, CH_2N, CH_2O), 4.25 (d, 1H, OCH_2), 4.51 (d, 1H, OCH_2), 7.06–7.62 (m, 15H, ArH). ^{13}C NMR (DMSO-d6): δ 55.4, 70.6, 70.7, 71.3, 77.0, 78.8, 127.0, 127.2, 127.6, 128.1, 128.4, 128.8, 128.9, 129.0, 139.4, 144.6, 145.3. ESI/MS (CH_3OH): m/z 388.0 $[M]^+$, Anal. calcd for $C_{26}H_{30}INO_2$: C 60.59, H 5.81, N 2.72, found: C 60.27, H 5.62, N 2.77.

4.1.5 | Synthesis of *N,N*-dimethyl-1-(2-methyl-6,6-diphenyl-1,4-dioxan-2-yl)methanamine (**9**)

A solution of **23** (2.3 mmol) and dimethylamine (10 mL) in dry benzene (15 mL) was heated in a sealed tube at 120°C for 60 h. The residue was dissolved in $CHCl_3$, which was washed with 2 N NaOH and dried over Na_2SO_4. The removal of the solvent gave a residue, which was purified by column chromatography, eluting with EtOAc to give an oil: 42% yield. ^{1}H NMR ($CDCl_3$): δ 0.89 (s, 3H, CH_3), 2.18–2.35 (m, 8H, CH_2, $N(CH_3)_2$), 3.42 (d, 1H, CH_2O), 3.65 (d, 1H, OCH_2), 3.75 (d, 1H, OCH_2), 4.41 (d, 1H, OCH_2), 7.16–7.43 (m, 10H, ArH). The free amine was transformed into the oxalate salt, which was recrystallized from 2-PrOH (mp 179–181°C). ^{13}C NMR (DMSO-d6): δ 21.9, 31.2, 46.4, 64.9, 72.0, 72.2, 73.3, 76.6, 126.0, 127.4, 127.6, 128.3, 128.4, 128.5, 144.9, 145.7, 164.3. ESI/MS (CH_3OH): *m/z* 312.3 $[M+H]^+$. Anal. calcd for $C_{20}H_{25}NO_2.C_2H_2O_4$: C 65.82, H 6.78, N 3.49, found: C 65.73, H 6.83, N 3.42.

The enantiomers (–)-**9** and (+)-**9** were separated by preparative chiral HPLC performed on the free amine (±)-**9** using a Phenomenex—Lux Cellulose-2 AXIA Pack (21.2 mm × 250 mm; particle size 5 µm) column as the chiral stationary phase and 100% *n*-hexane to *n*-hexane/2-PrOH:95/5 as the mobile phase (from 0 to 3 min linear increase of polarity from 100% *n*-hexane to *n*-hexane/2-PrOH:95/5, then isocratic elution until the end of the run at 30 min; Supporting Information S2: Figure S1) at a flow rate of 5 mL/min, with sample concentration of 5 mg/mL and injection volume of 4 mL. (+)-**9** eluted first ($[\alpha]^{20}_D$ = +40.8, c 1, $CHCl_3$), followed by (–)-**9** ($[\alpha]^{20}_D$ = –41.9, c 1, $CHCl_3$). The e.e., determined by analytical HPLC using a DAICEL—Chiralcel OZ-H (4.6 mm × 250 mm; particle size 5 µm) column as the chiral stationary phase and *n*-hexane/2-PrOH:95/5 as the mobile phase at a flow rate of 0.5 mL/min with a sample concentration of 1 mg/mL and injection volume of 20 µL, proved to be >98.5% for both enantiomers (chromatograms and t_R reported in Supporting Information S2: Figures S1 and S2).

4.1.6 | Synthesis of (*S*)-*N*,*N*-dimethyl-1-(2-methyl-6,6-diphenyl-1,4-dioxan-2-yl)methanamine [(*S*)-**9**]

This compound was prepared starting from (*R*)-**23** following the procedure described for **9**. An oil was obtained (55% yield). The ^{1}H NMR spectrum was identical to that of **9**. $[\alpha]^{20}_D$ = −41.6 (c 1, $CHCl_3$).

The free amine was transformed into the oxalate salt, which was recrystallized from 2-PrOH (mp 179–181°C). ESI/MS (CH_3OH): *m/z* 312.3 $[M + H]^+$. Anal. calcd for $C_{20}H_{25}NO_2.C_2H_2O_4$: C 65.82, H 6.78, N 3.49, found: C 65.63, H 6.70, N 3.42.

4.1.7 | Synthesis of (*R*)-*N*,*N*-dimethyl-1-(2-methyl-6,6-diphenyl-1,4-dioxan-2-yl)methanamine [(*R*)-**9**]

This compound was prepared starting from (*S*)-**23** following the procedure described for **9**. An oil was obtained (64% yield). The ^{1}H NMR spectrum was identical to that of **9**. $[\alpha]^{20}_D$ = + 40.9 (c 1, $CHCl_3$).

The free amine was transformed into the oxalate salt, which was recrystallized from 2-PrOH (mp 179-181°C). ESI/MS (CH_3OH): *m/z* 312.3 $[M + H]^+$. Anal. calcd for $C_{20}H_{25}NO_2.C_2H_2O_4$: C 65.82, H 6.78, N 3.49, found: C 65.70, H 6.88, N 3.52.

4.1.8 | Synthesis of *N*,*N*-dimethyl-1-(2-ethyl-6,6-diphenyl-1,4-dioxan-2-yl)methanamine (**10**)

This compound was prepared starting from **24** following the procedure described for **9**. An oil was obtained (46% yield). ^{1}H NMR ($CDCl_3$): δ 0.91 (t, 3H, CH_3), 1.42–1.73 (m, 2H, CH_2), 2.62 (s, 6H, $N(CH_3)_2$), 2.88 (s, 2H, CH_2N), 3.62 (d, 1H, CH_2O), 3.81 (d, 1H, OCH_2), 4.11 (d, 1H, OCH_2), 4.31 (d, 1H, OCH_2), 7.22–7.42 (m, 10H, ArH).

The free amine was transformed into the oxalate salt, which was recrystallized from 2-PrOH (mp 239–240°C). ^{13}C NMR (DMSO-d6): δ 8.8, 26.9, 34.7 47.2, 62.0, 69.4, 72.1, 76.3, 76.4, 126.4, 127.4, 127.5, 127.8, 128.3, 128.5, 145.4, 145.9, 163.8.

ESI/MS (CH_3OH): m/z 326.3 $[M + H]^+$, Anal. calcd for $C_{21}H_{27}NO_2.C_2H_2O_4$: C 66.49, H 7.04, N 3.37, found: C 66.19, H 7.22, N 3.48.

4.1.9 | Synthesis of *N*,*N*-dimethyl-1-(2,6,6-triphenyl-1,4-dioxan-2-yl)methanamine (**11**)

This compound was prepared starting from **25** following the procedure described for **9**. An oil was obtained (45% yield). The crude free amine was transformed into the oxalate salt, which was recrystallized from 2-PrOH (mp 182–183°C). ^{1}H NMR (CD_3OD): δ 3.21 (s, 6H, $N(CH_3)_2$), 3.42–3.68 (m, 4H, CH_2N, CH_2O), 4.42 (d, 1H, OCH_2), 4.96 (d, 1H, OCH_2), 7.22–7.83 (m, 15H, ArH). ^{13}C NMR (DMSO-d6): δ 31.1 46.8, 64.9, 71.4, 72.1, 75.1, 77.4, 126.0, 126.4, 127.4, 128.1, 128.3, 128.4, 128.9, 129.0, 141.3, 145.4, 145.5, 162.6. ESI/MS (CH_3OH): *m/z* 374.2 $[M + H]^+$. Anal. calcd for $C_{25}H_{27}NO_2.C_2H_2O_4$: C 69.96, H 6.31, N 3.02, found: C 69.65, H 6.27, N 3.13.

4.1.10 | Synthesis of 2-methylenebutan-1-ol (**12**)

A suspension of $LiAlH_4$ (3.0 mmol) in diethyl ether (20 mL) was added to a solution of 2-ethylacrolein (6.0 mmol) in diethyl ether (15 mL) at 0°C. The mixture was stirred for 10 min, and then EtOAc (1 mL) and silica were slowly added. After 20 min under stirring, the mixture was filtered and evaporated under a vacuum. An oil was obtained which was used without further purification. ^{1}H NMR ($CDCl_3$): δ 1.20 (t, 3H, CH_3), 1.80 (s, 1H, OH), 2.12 (q, 2H, CH_2), 4.09 (s, 2H, OCH_2), 4.75 (s, 1H, C=CH_2), 5.01 (s, 1H, C=CH_2).

4.1.11 | Synthesis of 2-phenylprop-2-en-1-ol (**13**)

CuI (3.0 mmol) was added to a solution of phenyl magnesium bromide (50 mmol) in diethyl ether (120 mL). The mixture was stirred for 0.5 h, and then a solution of propargyl alcohol (2 mmol) in diethyl ether (20 mL) was slowly added. Once the addition was complete, the reaction was refluxed for 24 h. After cooling, the mixture was washed with a saturated solution of NH_4Cl. The organic phase was separated, and the aqueous phase was extracted with diethyl ether. The organic phases were combined and dried over Na_2SO_4. After filtration and evaporation of the organic phase, the residue was purified by column chromatography, eluting with cyclohexane/EtOAc:1/10, to give an oil (72% yield). ^{1}H NMR ($CDCl_3$): δ 1.60 (s, 1H, OH), 4.58 (s, 2H, CH_2), 5.36 (s, 1H, C=CH_2), 5.68 (s, 1H, C=CH_2), 7.24 (m, 5H, ArH).

4.1.12 | Synthesis of ethyl 2-(2-methylenebutoxy) acetate (**14**)

NaH (23.2 mmol) was added to a solution of 2-methylenebutan-1-ol (**12**) (11.6 mmol) in THF (20 mL). After stirring for 15 min, a solution of ethyl 2-bromoacetate (13.9 mmol) in THF (20 mL) was added and the mixture was allowed to react at r.t. for 12 h. Then, it was poured into ice with a few drops of 12 N HCl and extracted with EtOAc. After filtration and evaporation of the organic phase, the residue was purified by column chromatography, eluting with cyclohexane/EtOAc:90/10, to give an oil (50% yield). ^{1}H NMR ($CDCl_3$): δ 1.05 (t, 3H, CH_3), 1.32 (t, 3H, CH_3), 2.12 (m, 2H, CH_2), 4.03 (s, 2H, CH_2), 4.04 (s, 2H, CH_2), 4.12 (m, 2H, CH_2), 4.91 (s, 1H, C=CH_2), 5.01 (s, 1H, C=CH_2).

4.1.13 | Synthesis of ethyl 2-[(2-phenylallyl)oxy] acetate (**15**)

This compound was prepared starting from **13** following the procedure described for **14**. An oil was obtained (48% yield). ^{1}H NMR ($CDCl_3$): δ 1.29 (t, 3H, CH_3), 4.12 (s, 2H, CH_2), 4.22 (m, 2H, CH_2), 4.50 (s, 2H, CH_2), 5.38 (s, 1H, C=CH_2), 5.61 (s, 1H, C=CH_2). 7.21–7.58 (m, 5H, ArH).

4.1.14 | Synthesis of 2-(2-methylenebutoxy)-1,1-diphenylethan-1-ol (**16**)

A solution of phenyl lithium in diethyl ether (1.9 M, 2 mL) was added to a solution of **14** (1.7 mmol) in THF (30 mL) at −78°C. The reaction mixture was stirred at r.t. for 30 min, then a saturated solution of NH_4Cl was added and the THF was evaporated. The residue was extracted with diethyl ether, washed with a saturated solution of NaCl, and dried over Na_2SO_4. After evaporation of the solvent, the residue was purified by column chromatography, eluting with cyclohexane/EtOAc:90/10 to give an oil (66% yield). ^{1}H NMR ($CDCl_3$): δ 1.04 (t, 3H, CH_3), 2.10 (m, 2H, CH_2), 3.95 (s, 2H, CH_2), 4.02 (m, 2H, CH_2), 4.81 (s, 1H, C=CH_2), 4.95 (s, 1H, C=CH_2), 7.21–7.42 (m, 10H, ArH).

4.1.15 | Synthesis of 1,1-diphenyl-2-[(2-phenylallyl)oxy]ethan-1-ol (**17**)

This compound was prepared starting from **15** (4.5 mmol) following the procedure described for **16**. An oil was obtained (43% yield). ^{1}H NMR ($CDCl_3$): δ 3.95 (s, 2H, CH_2), 4.52 (m, 2H, CH_2), 5.15 (s, 1H, C=CH_2), 5.58 (s, 1H, C=CH_2), 7.19-7.43 (m, 15H, ArH).

4.1.16 | Synthesis of 2-[(2-ethyloxiran-2-yl)methoxy]-1,1-diphenylethan-1-ol (**18**)

m-CPBA (46 mmol) was added in two portions to a solution of **16** (35 mmol) in dichloromethane (250 mL) at 0°C. After the acid was added, the mixture was left at r.t. for 20 h. The organic phase was washed with 10% Na_2SO_3 solution, 5% Na_2CO_3 solution, H_2O and then dried over Na_2SO_4. After evaporation of the solvent, the residue was purified by column chromatography, eluting with cyclohexane/EtOAc:95/5, to give an oil (86% yield). ^{1}H NMR ($CDCl_3$): δ 0.92 (t, 3H, CH_3), 1.56–1.80 (m, 2H, CH_2), 2.60 (dd, 2H, CH_2), 3.61 (d, 1H, CH_2), 3.72 (d, 1H, CH_2), 3.98 (d, 1H, CH_2), 4.18 (d, 1H, CH_2), 7.21-7.43 (m, 10H, ArH).

4.1.17 | Synthesis of 1,1-diphenyl-2-[(2-phenyloxiran-2-yl)methoxy]ethan-1-ol (**19**)

This compound was prepared starting from **17** (35 mmol) following the procedure described for **18**. An oil is obtained (41% yield). ^{1}H NMR ($CDCl_3$): δ 2.68 (d, 1H, CH_2), 3.01 (d, 1H, CH_2), 3.92 (d, 1H, CH_2), 3.98 (d, 1H, CH_2), 4.18 (d, 2H, CH_2), 7.11–7.53 (m, 15H, ArH).

4.1.18 | Synthesis of (*S*)-(2-methyl-6,6-diphenyl-1,4-dioxan-2-yl)methanol [(*S*)-**20**]

A solution of H_2O (0.035 mL) and $LiBH_4$ (0.6 mmol) in diethyl ether (10 mL) was added to a solution of [(*R*,*R*)-**26**] (0.6 mmol) in diethyl ether (50 mL) at 0°C. After 2 h at 0°C, 1 N NaOH (3 mL) was added. The mixture was extracted with EtOAc, which was dried over Na_2SO_4. The removal of the solvent afforded a residue that was purified by column chromatography, eluting with cyclohexane/EtOAc:90/10, to give a white solid: 60% yield; mp 114–115°C. ^{1}H NMR ($CDCl_3$): δ 1.12 (s, 3H, CH_3), 1.64 (br s, 1H, OH, exchangeable with D_2O), 3.35 (m, 2H, CH_2OH), 3.55 (d, 1H, CH_2O), 3.79 (d, 1H, CH_2O), 4.02 (d, 1H, CH_2O), 4.21 (d, 1H, CH_2O), 7.21–7.40 (m, 10H, ArH). $[\alpha]^{20}_D$ = -8.8 (c 1, $CHCl_3$).

4.1.19 | Synthesis of (*R*)-(2-methyl-6,6-diphenyl-1,4-dioxan-2-yl)methanol [(*R*)-**20**]

This compound was prepared starting from (*S*,*R*)-**26** following the procedure described for (*S*)-**20**. A white solid was obtained (58% yield, mp 114–115°C). The ^{1}H NMR spectrum was identical to that of (*S*)-**20**. $[\alpha]^{20}_D$ = +7.9 (c 1, $CHCl_3$).

4.1.20 | Synthesis of (2-ethyl-6,6-diphenyl-1,4-dioxan-2-yl)methanol (**21**)

A solution of **18** (3 mmol) and (1*S*)-(+)-10-CSA (0.17 mmol) in CH_2Cl_2 (70 mL) was refluxed for 8 h. The reaction mixture was then washed with a saturated solution of $NaHCO_3$ and dried over Na_2SO_4. The removal of the solvent gave a residue that was purified by column chromatography, eluting with cyclohexane/EtOAc:80/20, to afford an oil (47% yield). ^{1}H NMR ($CDCl_3$): δ 0.95 (t, 3H, CH_3), 1.55–1.74 (m, 2H, CH_2), 3.19 (d, 1H, CH_2OH), 3.38 (d, 1H, CH_2OH), 3.60 (d, 1H, CH_2O), 3.64 (m, 2H, CH_2O), 4.51 (d, 1H, CH_2O), 7.20–7.44 (m, 10H, ArH).

4.1.21 | Synthesis of (2,6,6-triphenyl-1,4-dioxan-2-yl)methanol (**22**)

This compound was prepared starting from **19** following the procedure described for **21**. An oil was obtained (25% yield). ^{1}H NMR ($CDCl_3$): δ 1.41 (br s, 1H, OH), 3.55 (m, 2H, CH_2), 3.69 (d, 1H, CH_2O), 3.78 (d, 1H, CH_2O), 4.20 (d, 1H, CH_2O), 3.71 (d, 1H, CH_2O), 7.10-7.60 (m, 15H, ArH).

4.1.22 | Synthesis of (2-methyl-6,6-diphenyl-1,4-dioxan-2-yl)methyl 4-methylbenzenesulfonate (**23**)

p-Tosyl chloride (7.0 mmol) was added to a stirred solution of **20** (6.0 mmol) in pyridine (5 mL) at 0°C over 30 min. After 3 h at 0°C, the mixture was left for 20 h at 4°C in the freezer. Then it was poured into ice and 12 N HCl (5 mL) and extracted with $CHCl_3$. The organic layers were washed with 2 N HCl (15 mL), $NaHCO_3$ saturated solution (15 mL), H_2O (15 mL), and then dried over Na_2SO_4. The evaporation of the solvent afforded a residue that was purified by

column chromatography, eluting with petroleum ether/EtOAc:80/20 to give a white solid: 43% yield, mp 118–120°C. ^{1}H NMR ($CDCl_3$): δ 1.18 (s, 3H, CH_3), 2.42 (s, 3H, CH_3), 3.38 (m, 2H, CH_2O), 3.60 (d, 1H, CH_2O), 3.71 (m, 2H, CH_2O), 4.32 (d, 1H, CH_2O), 7.18–7.58 (m, 14H, ArH).

4.1.23 | Synthesis of (*R*)-(2-methyl-6,6-diphenyl-1,4-dioxan-2-yl)methyl 4-methylbenzenesulfonate [(*R*)-(**23**)]

This compound was prepared starting from (*S*)-**20** following the procedure described for **23**. A white solid was obtained: 51% yield; mp 118-120°C. The ^{1}H NMR spectrum was identical to that of **23**. $[\alpha]^{20}_D$ = −64.2 (c 1, $CHCl_3$).

4.1.24 | Synthesis (*S*)-(2-methyl-6,6-diphenyl-1,4-dioxan-2-yl)methyl 4-methylbenzenesulfonate [(*S*)-(**23**)]

This compound was prepared starting from (*R*)-**20** following the procedure described for **23**. A white solid was obtained: 55% yield; mp 118–120°C. The ^{1}H NMR spectrum was identical to that of **23**. $[\alpha]^{20}_D$ = +65.9 (c 1, $CHCl_3$).

4.1.25 | Synthesis of (2-ethyl-6,6-diphenyl-1,4-dioxan-2-yl)methyl 4-methylbenzenesulfonate (**24**)

This compound was prepared starting from **21** following the procedure described for **23**. A white solid was obtained: 71% yield; mp 137–139°C. ^{1}H NMR ($CDCl_3$): δ 0.95 (t, 3H, CH_3), 1.48–1.65 (m, 2H, CH_2), 2.43 (s, 3H, CH_3), 3.25 (d, 1H, CH_2O), 3.40 (d, 1H, CH_2O), 3.48 (d, 2H, CH_2O), 3.78 (d, 1H, CH_2O), 4.51 (d, 1H, CH_2O), 7.18–7.42 (m, 14H, ArH).

4.1.26 | Synthesis of (2,6,6-triphenyl-1,4-dioxan-2-yl)methyl 4-methylbenzenesulfonate (**25**)

This compound was prepared starting from **22** following the procedure described for **23**. A white solid was obtained: 64% yield; mp 129–130°C. ^{1}H NMR ($CDCl_3$): δ 2.41 (s, 3H, CH_3), 3,42 (d, 1H, CH_2O), 3.61 (d, 1H, CH_2O), 3.82 (m, 2H, CH_2O), 4.31 (d, 1H, CH_2O), 4.62 (d, 1H, CH_2O), 7.15-7.51 (m, 19H, ArH).

4.2 | Binding assays

4.2.1 | Cell culture and membrane preparation

CHO-K1 cells stably transfected with $hM_{1\text{-}5}$ receptor subtypes were generously provided by Prof. R. Maggio (Department of Biotechnological and Applied Clinical Sciences, University of L'Aquila, Italy).[45] Cells were grown in Dulbecco's Modified Eagle's Medium (DMEM) with nutrient mixture F12 (DMEM/F12, 50/50), containing 10% fetal bovine serum, penicillin (100 U/mL), streptomycin (100 U/mL), L-glutamine (4 mM), and geneticin (G-418, 50 µg/mL) at 37°C in 5% CO_2 umidified incubator. To harvest the cells, the culture medium was removed, the cells were washed with PBS then trypsinized by trypsin-EDTA treatment for 2–3 min. A total of 0.7 mL of serum was added to inactivate the trypsin and the cells were spun down by centrifuging at 300*g* for 5 min. The cells were then resuspended in ice-cold 25 mM sodium phosphate buffer containing 5 mM $MgCl_2$, pH 7.4 (binding buffer) and homogenized using a cell disrupter (Ultra-Turrax, setting 3, 30 s). The homogenate was sedimented by centrifugation (17,000*g*, 15 min). The supernatant was discarded and the resulting pellets were resuspended with Ultra-Turrax in the same buffer to give a final protein concentration of 1–2 mg/mL. Protein content was determined by the method of Bradford (1976) with bovine serum albumin (Sigma) as a standard and stored at −80°C.

4.2.2 | Inhibition radioligand binding assay

Inhibition radioligand binding assays were conducted as previously described[46,47] with 0.2 nM [^{3}H]NMS (Perkin-Elmer Life and Analytical Science, SA 84 Ci/mmol) in binding buffer in a final volume of 250 µL. Nonspecific binding was defined in the presence of 10 µM atropine. Briefly, the cell homogenates (about 25–70 µg/mL of protein) were incubated with radioligand and unlabeled test compounds for 2 h at room temperature. Bound and free radioactivity were separated by filtering the assay mixture through Unifilter GF/B plates using a FilterMate Cell Harvester (Perkin-Elmer Life and Analytical Science). The filter-bound radioactivity was counted by TopCount NXT Microplate Scintillation Counter (Perkin-Elmer Life and Analytical Science). Data (cpm) were normalized to percentage-specific binding and analyzed using a four-parameter logistic equation in GraphPad Prism 5.02; IC_{50} values were determined and K_i values were calculated.[48] The values reported in Tables 1 and 2 represent the arithmetic mean ± S.E.M. of at least four to eight independent experiments, each one performed in duplicate. The radioligand displacement curves from competition binding assays for compound (±)-**9** are shown in Figure 3 and those of compounds **6**-**8**, (*S*)-(−)-**9**, (*R*)-(+)-**9**, **10**, and **11** are shown in Supporting Information S2: Figures S12-S18.

4.3 | Computational studies

4.3.1 | Molecular docking

Molecular docking was performed by means of the software PLANTS[49] by using the crystal structure of human M_1 receptor in complex with the antagonist tiotropium (PDB ID 5CXV).[43]

Hydrogens were added to the protein by means of UCSF ChimeraX.[50] The structure was optimized by 10,000 steps of energy minimization by keeping the backbone fixed to preserve the original folding. Ligand structures were prepared as described elsewhere.[51] The binding site was defined to include all the residues within 10 Å from the co-crystallized ligand. Ten poses were computed for each ligand using speed 1 as the search mode and ChemPLP as the scoring function.

4.3.2 | MD

MD simulations were performed by means of Amber18.[52] CHARMM-gui webserver (https://www.charmm-gui.org/)[53] was used to set up the simulation and generate the initial input files. Each system was embedded in a bilayer composed of 70% phosphatidylcholine and 30% cholesterol, solvated in a rectangular box of TIP3P water molecules, and neutralized with NaCl setting a salt concentration of 0.15 M. The General Amber Force Field (GAFF)[54] was used for ligands parametrization, while ff14SB[55] and lipid17 were employed to parametrize the protein and the membrane, respectively. Each system was subjected to 2500 steps minimization using the steepest descent algorithm followed by 2500 steps of conjugate gradient minimization applying positional restraints on the protein–ligand complex (10 kcal·mol^{-1} · Å^{-2}) and on the membrane (2.5 kcal·mol^{-1} · Å^{-2}). Subsequently, 125 ps heating phase was performed by increasing the temperature to 300 K exploiting the Langevin thermostat, and keeping the same positional restraints applied during minimization. Two equilibration phases were performed, first using the NVT ensemble for 125 ps and reducing the restraints on the protein–ligand complex (5 kcal·mol^{-1} · Å^{-2}), and then employing the NPT ensemble for 1.625 ns keeping the pressure around 1 atm by means of the Berendsen barostat and gradually reducing the weight of the restraints. A production run of 300 ns was carried out at constant pressure without any restraint using a timestep of 2 fs. All bonds involving hydrogen atoms were restrained by the SHAKE algorithm. The Particle-Mesh Ewald (PME) method was used to compute electrostatic interactions and periodic boundary conditions were applied. The Cpptraj module[56] of AmberTools 18 was used for RMSD and cluster analysis which was performed basing on the heavy atoms RMSD of the ligand by using the average linkage hierarchical agglomerative method implemented in Cpptraj, setting an epsilon value of 1.5. Interaction fingerprints were computed at intervals of 15 frames using the ProLIF Python library[57] and converted into an interaction fraction by dividing the number of frames exhibiting a given interaction by the total number of frames. In this analysis, only interactions appearing for at least 30% of the simulation time were considered.

ACKNOWLEDGMENTS

This work was supported by the Unione Europea-Next generation EU, "MUR fondo promozione e sviluppo-DM737/2001, INVIRCuM and PROCARAPINE", (University of Camerino, FAR 2022, PNR) and the National Institute on Drug Abuse, Intramural Research Program (NIDA-IRP; A.B.). Open access publishing facilitated by Universita degli Studi di Camerino, as part of the Wiley - CRUI-CARE agreement.

CONFLICTS OF INTEREST STATEMENT

The authors declare no conflicts of interest.

DATA AVAILABILITY STATEMENT

The data that support the findings of this study are available from the corresponding author upon reasonable request.

ORCID

Wilma Quaglia http://orcid.org/0000-0002-7708-0200
Fabio Del Bello http://orcid.org/0000-0001-6538-6029

REFERENCES

[1] T. Haga, *Proc. Japan Acad. Series B* **2013**, *89*, 226.
[2] D. A. Brown, *J. Mol. Neurosci.* **2010**, *41*, 340.
[3] E. C. Hulme, N. J. M. Birdsall, N. J. Buckley, *Annu. Rev. Pharmacol. Toxicol.* **1990**, *30*, 633.
[4] P. Abrams, K. E. Andersson, *BJU Int.* **2007**, *100*, 987.
[5] M. G. Matera, P. Rogliani, M. Cazzola, *Expert Opin. Pharmacother.* **2014**, *15*, 961.
[6] M. Cazzola, J. Ora, P. Rogliani, M. G. Matera, *Expert Rev. Respir. Med.* **2017**, *11*, 239.
[7] D. J. Foster, Z. K. Bryant, P. J. Conn, *Behav. Brain Res.* **2021**, *405*, 113201.
[8] D. Dencker, M. Thomsen, G. Wörtwein, P. Weikop, Y. Cui, J. Jeon, J. Wess, A. Fink-Jensen, *ACS Chem. Neurosci.* **2012**, *3*, 80.
[9] H. Hampel, M. M. Mesulam, A. C. Cuello, M. R. Farlow, E. Giacobini, G. T. Grossberg, A. S. Khachaturian, A. Vergallo, E. Cavedo, P. J. Snyder, Z. S. Khachaturian, *Brain* **2018**, *141*, 1917.
[10] E. R. Spindel, *Handb. Exp. Pharmacol.* **2012**, *208*, 451.
[11] L. Zhu, M. Rossi, N. M. Doliba, J. Wess, *Int. Immunopharmacol.* **2020**, *81*, 106267.
[12] A. Y. Deng, D. Deblois, S. A. Laporte, D. Gelinas, J. C. Tardif, E. Thorin, Y. Shi, A. Raignault, A. Ménard, *Hypertension* **2018**, *72*, 755.
[13] F. De Angelis, A. Maria Tata, *Cent. Nerv. Syst. Agents Med. Chem.* **2016**, *16*, 218.
[14] I. Wessler, C. J. Kirkpatrick, *Int. Immunopharmacol.* **2020**, *83*, 106345.
[15] C. M. Marson *Heterocyclic Chemistry in the 21st Century - A Tribute to Alan Katritzky*, (Eds: E. F. V. Scriven, C. A. Ramsden), Academic Press, **2017**, *121*, p. 13.
[16] J. Jampilek, *Molecules* **2019**, *24*, 3839.
[17] T. J. Ritchie, S. J. F. Macdonald, S. Peace, S. D. Pickett, C. N. Luscombe, *MedChemComm* **2012**, *3*, 1062.
[18] K. J. Broadley, D. R. Kelly, *Molecules* **2001**, *6*, 142.
[19] W. Quaglia, A. Piergentili, F. Del Bello, Y. Farande, M. Giannella, M. Pigini, G. Rafaiani, A. Carrieri, C. Amantini, R. Lucciarini, G. Santoni, E. Poggesi, A. Leonardi, *J. Med. Chem.* **2008**, *51*, 6359.
[20] V. Mammoli, A. Bonifazi, F. Del Bello, E. Diamanti, M. Giannella, A. L. Hudson, L. Mattioli, M. Perfumi, A. Piergentili, W. Quaglia, F. Titomanlio, M. Pigini, *Bioorg. Med. Chem.* **2012**, *20*, 2259.
[21] A. Bonifazi, A. Piergentili, F. Del Bello, Y. Farande, M. Giannella, M. Pigini, C. Amantini, M. Nabissi, V. Farfariello, G. Santoni, E. Poggesi, A. Leonardi, S. Menegon, W. Quaglia, *J. Med. Chem.* **2013**, *56*, 584.
[22] A. Bonifazi, F. Del Bello, V. Mammoli, A. Piergentili, R. Petrelli, C. Cimarelli, M. Pellei, D. Schepmann, B. Wünsch, E. Barocelli, S. Bertoni, L. Flammini, C. Amantini, M. Nabissi, G. Santoni, G. Vistoli, W. Quaglia, *J. Med. Chem.* **2015**, *58*, 8601.

[23] F. Del Bello, A. Bonifazi, M. Giannella, G. Giorgioni, A. Piergentili, R. Petrelli, C. Cifani, M. V. Micioni Di Bonaventura, T. M. Keck, A. Mazzolari, G. Vistoli, A. Cilia, E. Poggesi, R. Matucci, W. Quaglia, *Eur. J. Med. Chem.* **2017**, *125*, 233.
[24] F. Del Bello, A. Bonifazi, G. Giorgioni, W. Quaglia, C. Amantini, M. B. Morelli, G. Santoni, F. O. Battiti, G. Vistoli, A. Cilia, A. Piergentili, *Eur. J. Med. Chem.* **2019**, *168*, 461.
[25] M. B. Morelli, C. Amantini, M. Nabissi, G. Santoni, B. Wünsch, D. Schepmann, C. Cimarelli, M. Pellei, C. Santini, S. Fontana, V. Mammoli, W. Quaglia, A. Bonifazi, M. Giannella, G. Giorgioni, A. Piergentili, F. Del Bello, *ACS Med. Chem. Lett.* **2019**, *10*, 511.
[26] F. Del Bello, D. Ambrosini, A. Bonifazi, A. H. Newman, T. M. Keck, M. Giannella, G. Giorgioni, A. Piergentili, L. Cappellacci, A. Cilia, S. Franchini, W. Quaglia, *ACS Chem. Neurosci.* **2019**, *10*, 2222.
[27] A. Bonifazi, A. H. Newman, T. M. Keck, S. Gervasoni, G. Vistoli, F. Del Bello, G. Giorgioni, P. Pavletić, W. Quaglia, A. Piergentili, *ACS Chem. Neurosci.* **2021**, *12*, 3638.
[28] A. Piergentili, W. Quaglia, M. Giannella, F. D. Bello, B. Bruni, M. Buccioni, A. Carrieri, S. Ciattini, *Bioorg. Med. Chem.* **2007**, *15*, 886.
[29] A. Piergentili, W. Quaglia, M. Giannella, F. Del Bello, M. Buccioni, M. Nesi, R. Matucci, *Bioorg. Med. Chem. Lett.* **2008**, *18*, 614.
[30] A. Piergentili, W. Quaglia, F. D. Bello, M. Giannella, M. Pigini, E. Barocelli, S. Bertoni, R. Matucci, M. Nesi, B. Bruni, *Bioorg. Med. Chem.* **2009**, *17*, 8174.
[31] F. Del Bello, E. Barocelli, S. Bertoni, A. Bonifazi, M. Camalli, G. Campi, M. Giannella, R. Matucci, M. Nesi, M. Pigini, W. Quaglia, A. Piergentili, *J. Med. Chem.* **2012**, *55*, 1783.
[32] F. Del Bello, A. Bonifazi, G. Giorgioni, R. Petrelli, W. Quaglia, A. Altomare, A. Falcicchio, R. Matucci, G. Vistoli, A. Piergentili, *Eur. J. Med. Chem.* **2017**, *137*, 327.
[33] F. Del Bello, A. Bonifazi, G. Giorgioni, A. Piergentili, M. G. Sabbieti, D. Agas, M. Dell'aera, R. Matucci, M. Górecki, G. Pescitelli, G. Vistoli, W. Quaglia, *J. Med. Chem.* **2020**, *63*, 5763.
[34] A. Choppin, R. M. Eglen, *Br. J. Pharmacol.* **2001**, *132*, 835.
[35] G. Marucci, A. Piero, L. Brasili, M. Buccioni, D. Giardinà, U. Gulini, A. Piergentili, G. Sagratini, *Med. Chem. Res.* **2005**, *14*, 274.
[36] G. K. Jahangiri, J.-L. Reymond, *J. Am. Chem. Soc.* **1994**, *116*, 11264.
[37] Z.-C. Duan, X.-P. Hu, C. Zhang, D.-Y. Wang, S.-B. Yu, Z. Zheng, *J. Org. Chem.* **2009**, *74*, 9191.
[38] V. Avlani, L. T. May, P. M. Sexton, A. Christopoulos, *J. Pharmacol. Exp. Ther.* **2004**, *308*, 1062.
[39] S. Marsango, R. J. Ward, E. Alvarez-Curto, G. Milligan, *Neuropharmacology* **2018**, *136*, 401.
[40] J. C. Goin, N. M. Nathanson, *J. Biol. Chem.* **2006**, *281*, 5416.
[41] P. S. H. Park, J. W. Wells, *Biochemistry* **2003**, *42*, 12960.
[42] S. M. Mcmillin, M. Heusel, T. Liu, S. Costanzi, J. Wess, *J. Biol. Chem.* **2011**, *286*, 28584.
[43] D. M. Thal, B. Sun, D. Feng, V. Nawaratne, K. Leach, C. C. Felder, M. G. Bures, D. A. Evans, W. I. Weis, P. Bachhawat, T. S. Kobilka, P. M. Sexton, B. K. Kobilka, A. Christopoulos, *Nature* **2016**, *531*, 335.
[44] S. Vittorio, R. Gitto, I. Adornato, E. Russo, L. De Luca, *Molecules* **2021**, *26*, 1103.
[45] R. Maggio, P. Barbier, M. L. Bolognesi, A. Minarini, D. Tedeschi, C. Melchiorre, *Eur. J. Pharmacol. Mol. Pharmacol.* **1994**, *268*, 459.
[46] F. Del Bello, A. Bonifazi, G. Giorgioni, C. Cifani, M. V. Micioni Di Bonaventura, R. Petrelli, A. Piergentili, S. Fontana, V. Mammoli, H. Yano, R. Matucci, G. Vistoli, W. Quaglia, *J. Med. Chem.* **2018**, *61*, 3712.
[47] A. Bonifazi, H. Yano, F. Del Bello, A. Farande, W. Quaglia, R. Petrelli, R. Matucci, M. Nesi, G. Vistoli, S. Ferré, A. Piergentili, *J. Med. Chem.* **2014**, *57*, 9065.
[48] Y. Cheng, W. H. Prusoff, *Biochem. Pharmacol.* **1973**, *22*, 3099.
[49] O. Korb, T. Stützle, T. E. Exner, *PLANTS: Application of Ant Colony Optimization to Structure-Based Drug Design*, Paper presented at the Ant Colony Optimization and Swarm Intelligence, Berlin, Heidelberg **2006**.
[50] E. C. Meng, T. D. Goddard, E. F. Pettersen, G. S. Couch, Z. J. Pearson, J. H. Morris, T. E. Ferrin, *Protein Sci.* **2023**, *32*, e4792.
[51] D. Moi, S. Vittorio, A. Angeli, G. Balboni, C. T. Supuran, V. Onnis, *Molecules* **2022**, *28*, 91.
[52] D. A. Case, T. E. Cheatham, 3rd, T. Darden, H. Gohlke, R. Luo, K. M. Merz, Jr., A. Onufriev, C. Simmerling, B. Wang, R. J. Woods, *J. Comput. Chem.* **2005**, *26*, 1668.
[53] S. Jo, T. Kim, V. G. Iyer, W. Im, *J. Comput. Chem.* **2008**, *29*, 1859.
[54] J. Wang, R. M. Wolf, J. W. Caldwell, P. A. Kollman, D. A. Case, *J. Comput. Chem.* **2004**, *25*, 1157.
[55] J. A. Maier, C. Martinez, K. Kasavajhala, L. Wickstrom, K. E. Hauser, C. Simmerling, *J. Chem. Theory Comput.* **2015**, *11*, 3696.
[56] D. R. Roe, T. E. Cheatham, 3rd, *J. Chem. Theory Comput.* **2013**, *9*, 3084.
[57] C. Bouysset, S. Fiorucci, *J. Cheminf.* **2021**, *13*, 72.

SUPPORTING INFORMATION

Additional supporting information can be found online in the Supporting Information section at the end of this article.

How to cite this article: G. Giorgioni, A. Bonifazi, R. Matucci, F. Matteucci, A. Piergentili, A. Piergentili, W. Quaglia, S. Gervasoni, G. Vistoli, S. Vittorio, F. Del Bello, *Arch. Pharm.* **2024**;*357*:e2400337. https://doi.org/10.1002/ardp.202400337